NeuroImage: Clinical 27 (2020) 102338

Contents lists available at ScienceDirect

NeuroImage: Clinical

journal homepage: www.elsevier.com/locate/ynicl

Applying surface-based morphometry to study ventricular abnormalities of cognitively unimpaired subjects prior to clinically significant memory decline

Qunxi Dong[a,1], Wen Zhang[a,1], Cynthia M. Stonnington[b], Jianfeng Wu[a], Boris A. Gutman[c], Kewei Chen[d], Yi Su[d], Leslie C. Baxter[e], Paul M. Thompson[f], Eric M. Reiman[d], Richard J. Caselli[g], Yalin Wang[a,*]

[a] School of Computing, Informatics, and Decision Systems Engineering, Arizona State University, Tempe, AZ, USA
[b] Department of Psychiatry and Psychology, Mayo Clinic, Scottsdale, AZ, USA
[c] Armour College of Engineering, Illinois Institute of Technology, Chicago, IL, USA
[d] Banner Alzheimer's Institute, Phoenix, AZ, USA
[e] Human Brain Imaging Laboratory, Barrow Neurological Institute, Phoenix, AZ, USA
[f] Imaging Genetics Center, Institute for Neuroimaging and Informatics, University of Southern California, Los Angeles, CA, USA
[g] Department of Neurology, Mayo Clinic Arizona, Scottsdale, AZ, USA

ARTICLE INFO

Keywords:
Alzheimer's disease
Cognitively unimpaired subjects
Memory decline
Ventricular surface
Multivariate tensor-based morphometry
Ventricular abnormalities

ABSTRACT

Ventricular volume (VV) is a widely used structural magnetic resonance imaging (MRI) biomarker in Alzheimer's disease (AD) research. Abnormal enlargements of VV can be detected before clinically significant memory decline. However, VV does not pinpoint the details of subregional ventricular expansions. Here we introduce a ventricular morphometry analysis system (VMAS) that generates a whole connected 3D ventricular shape model and encodes a great deal of ventricular surface deformation information that is inaccessible by VV. VMAS contains an automated segmentation approach and surface-based multivariate morphometry statistics. We applied VMAS to two independent datasets of cognitively unimpaired (CU) groups. To our knowledge, it is the first work to detect ventricular abnormalities that distinguish normal aging subjects from those who imminently progress to clinically significant memory decline. Significant bilateral ventricular morphometric differences were first shown in 38 members of the *Arizona APOE* cohort, which included 18 CU participants subsequently progressing to the clinically significant memory decline within 2 years after baseline visits (progressors), and 20 matched CU participants with at least 4 years of post-baseline cognitive stability (non-progressors). VMAS also detected significant differences in bilateral ventricular morphometry in 44 Alzheimer's Disease Neuroimaging Initiative (ADNI) subjects (18 CU progressors vs. 26 CU non-progressors) with the same inclusion criterion. Experimental results demonstrated that the ventricular anterior horn regions were affected bilaterally in CU progressors, and more so on the left. VMAS may track disease progression at subregional levels and measure the effects of pharmacological intervention at a preclinical stage.

1. Introduction

Alzheimer's disease (AD) is the most prevalent neurodegenerative disease. By 2050, 1 in 85 persons worldwide will be living with it, which will consume enormous social resources (Brookmeyer et al. 2007). Failure of clinical trials in symptomatic patients has led to the belief that capturing brain changes and intervening at preclinical stages would more likely achieve therapeutic success (Brookmeyer et al. 2007; Sperling et al. 2011a). Advances in neuroimaging biomarkers based on positron emission tomography (PET), structural magnetic resonance imaging (MRI) and cerebral spinal fluid (CSF) imaging methods (Sperling et al. 2011a; Jack et al. 2016) provide evidence of AD pathophysiology in vivo. Structural MRI biomarkers are the mainstay of AD imaging research as well as clinical diagnosis (Sperling et al. 2011b;

* Corresponding author at: School of Computing, Informatics, and Decision Systems Engineering, Arizona State University, P.O. Box 878809, Tempe, AZ 85287 USA.
E-mail address: ylwang@asu.edu (Y. Wang).
[1] Authors contributed equally

https://doi.org/10.1016/j.nicl.2020.102338
Received 19 March 2020; Received in revised form 15 June 2020; Accepted 2 July 2020
Available online 05 July 2020

Tosun et al. 2016). MRI biomarkers include whole-brain (Chen et al. 2007; Frisoni et al. 2010; Cuingnet et al. 2011), entorhinal cortex (Cardenas et al. 2011; Zhou et al. 2013; Li et al. 2014), hippocampus (Reiman et al. 1998; Pardoe et al. 2009; Shi et al. 2013a; Li et al.,2016; Saeed et al. 2018; Dong et al. 2019), and temporal lobe volumes (Hua et al. 2010; Coupé et al. 2019), as well as ventricular expansion (Jack et al., 2008; Thompson et al., 2006; Wang et al., 2011). Ventricular expansion reflects diffuse brain atrophy (Madsen et al., 2013, 2015). Owing to the high contrast between the CSF and surrounding brain tissue on T1-weighted images, the lateral ventricles can be measured more reliably than other brain structures (Chou et al. 2010). These ventricular characteristics make ventricular expansion measures detectable at early and potentially preclinical AD stages (Apostolova et al. 2012; Roussotte et al. 2014a).

Ventricular expansion can be described by ventricular volume (VV) (Weiner 2008; Roussotte et al. 2014b, a; Madsen et al. 2015; Coupé et al. 2019) and ventricular surface morphometry (Thompson et al. 2004a; Wang et al. 2010; Gutman et al. 2013; Shi et al. 2015). Accelerating VV is associated with AD-related neuropathological progression and can be detected prior to clinically significant memory decline (Weiner 2008; Apostolova et al. 2012; Roussotte et al. 2014a; Madsen et al. 2015; Coupé et al. 2019). However, with VV alone cannot pinpoint the deformation details at the sub-regional level. We propose that ventricular morphology offers the possibility of being a more sensitive indicator of the details of subregional ventricular expansions which may differ between clinical subgroups.

Surface-based ventricular morphology biomarkers derived from ventricular anatomical models, such as radial distances (RD, distances from the medial core to each surface point) (Thompson et al. 2004a; Ferrarini et al. 2006) and tensor-based morphometry (TBM) (Chung et al., 2003, 2008; Shi et al. 2015), are useful in overcoming partial volume effects and identifying detailed point-wise correlations between structural deformations and neurodegenerative progression of AD. RDs were estimated in order to track subfield morphology along the ventricular surface normal directions (Thompson et al. 2004a; Wang et al. 2011; Apostolova et al. 2012; Gutman et al. 2013; Roussotte et al. 2014b, a). Deformations of ventricular subfields associated with cognitive decline can be located and visualized using a 3D RD field (Thompson et al. 2004a). With the help of RD mapping, age related expansions of frontal and body/occipital horn portions of the lateral ventricles were found in cognitively unimpaired (CU) subjects (Apostolova et al. 2012). Radial expansion of ventricular temporal horn surfaces was faster in AD than in CU subjects (Thompson et al. 2004a).

Surface TBM (Thompson et al. 2000; Chung et al., 2003, 2008) is able to quantify brain deformations within surfaces. It has been applied to detect regional differences in brain surface morphometry between clinical groups (Shi et al. 2015). However, TBM is limited in its accuracy of modeling relatively small-scale structures (Chou et al. 2008). To overcome this limitation, we developed the multivariate TBM (mTBM) method and applied it to HIV/AIDS subjects and healthy controls (Wang et al. 2010). This method gave better effect sizes for detecting ventricular morphometry differences than other TBM-based methods, including analysis of the Jacobian determinant, the largest and smallest eigenvalues of the surface metric, and the pair of eigenvalues of the Jacobian matrix (Wang et al. 2010, 2011). To comprehensively capture deformations along the surface normal directions and within surfaces, we developed multivariate morphometry statistics (MMS) combining mTBM and RD to detect brain abnormalities associated with neurodegenerative diseases (Dong et al., 2019; Shi et al., 2014, 2015; Wang et al., 2011; Li et al.,2016). Our previous studies (Wang et al. 2010, 2011) demonstrated that surface-based MMS gained improved statistical power compared to other TBM-based methods.

Few studies have revealed ventricular morphometry abnormalities of CU progressors who imminently progressed to clinically significant memory decline. Previous studies of ventricular morphometric modeling (Thompson et al. 2004a; Ferrarini et al. 2008; Chou et al. 2008; Wang et al. 2011; Apostolova et al. 2012; Roussotte et al. 2014b) mapped only part of anatomical ventricular surfaces, with coverage of inferior or posterior horns being incomplete. In this work, we propose a complete ventricular morphometry analysis system (VMAS), which is based on MMS proposed by our previous methods (Wang et al. 2010, 2011), but includes an automated ventricular segmentation method (Zhang et al. 2016), together with an efficient morphometric expansion/atrophy visualization analysis module (Yao et al. 2018; Dong et al. 2019). The proposed VMAS can capture a whole connected 3D ventricular surface characteristic as well as subregional deformations. We hypothesize that our VMAS will detect and visualize ventricular morphometry abnormalities of CU progressors who subsequently progressed to clinically significant memory decline within 2 years post-baseline, compared to CU non-progressors. We test and validate this hypothesis in two independent CU cohorts, using cross-sectional structural MRI and the VMAS to compute bilateral ventricular morphometries and visualize ventricular morphometric expansions at subregional levels that are related to memory decline.

2. Materials and methods

2.1. Subjects

Two cohorts were used for testing the performance of the VMAS. The first is the *Arizona APOE cohort*: 38 subjects from an imaged subcohort of 280 drawn from the 26-year longitudinal *Arizona APOE* cohort study (Caselli et al. 2004, 2009). The subjects selection met the criterion adopted in our prior work (Stonnington et al. 2018): CU progressors had both MRI and FDG PET data while still cognitively unimpaired at the epoch approximately 2 years prior to progression to clinically memory impairment; CU non-progressors had at least 4 years over which they remained cognitively unimpaired and matched to progressors for sex, age, education and APOE allele dose. Then we found 18 CU progressors and matched 20 CU non-progressors in the Arizona APOE cohort. Among these 18 progressors, sixteen were eventually diagnosed with amnestic mild cognitive impairment (aMCI), one with amnestic and visuospatial MCI, and one with mild stage AD dementia. AMCI diagnosis fulfilled published criteria (Albert et al. 2011; McKhann et al. 2011). The *Arizona APOE* cohort was approved by the Mayo Clinic and Banner Good Samaritan Institutional Review Boards. After a complete description of the study was given to the subjects, written informed consent was obtained.

The second cohort is drawn from the *Alzheimer's Disease Neuroimaging Initiative (ADNI) database* (adni.loni.usc.edu). ADNI is the result of efforts of many co-investigators from a broad range of academic institutions and private corporations. Subjects have been recruited from over 50 sites across the U.S. and Canada. The primary goal of ADNI is to test whether biological markers, such as serial MRI and PET, combined with clinical and neuropsychological assessments, can measure the progression of MCI and early AD. Subjects originally recruited for ADNI-1 and ADNI-GO had the option to be followed in ADNI-2. For up-to-date information, see www.adni-info.org. In this study, study participants were drawn from ADNI-1 data base utilizing the same inclusion criteria described above for the Arizona APOE cohort. From ADNI-1, we found 18 participants who developed clinically significant memory impairment, i.e. aMCI, in approximately 2 years and 26 age, sex, education and APOE-matched non-progressors remained cognitively unimpaired for at least 4 years.

2.2. Overview of VMAS

The current work proposes the VMAS to study the ventricular abnormalities of CU progressors compared to CU non-progressors during the preclinical stage, as shown in Fig. 1. This system consists of ventricular segmentation, ventricular surface reconstruction, and ventricular surface MMS analysis.

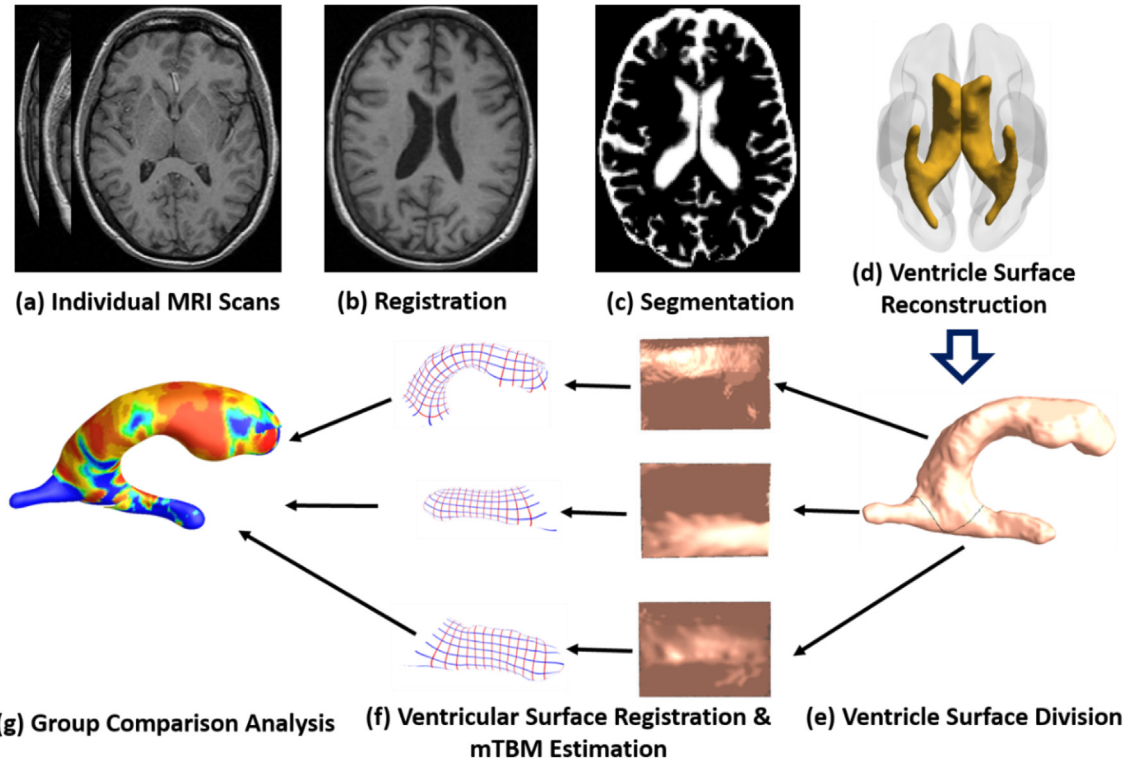

Fig. 1. An illustration of the novel surface-based ventricular morphometry analysis system. First, individual MRI scans (a) were linearly registered into a standard space (MNI152) (b). Second, the registered images were segmented into three brain tissue types (the gray matter, white matter, and CSF); a group-wise CSF template was created from all individual CSF masks, and the group-wise ventricular template were subsequently obtained from the group-wise CSF template (c). Third, binary ventricular masks were segmented and extracted, then ventricular surface meshes were constructed and smoothed (d). Fourth, the whole ventricular surface was cut into three sub-structures (e). Fifth, each sub-ventricular surface was conformally mapped to a rectangle in the parameter domain, and vertex-wise multivariate morphometry statistics (MMS) were estimated on these mapped surfaces (f). Last, the morphometric variations of ventricular surfaces between groups were evaluated, and significantly different subregions were shown in the form of a *p*-map (non-blue regions: $p < 0.05$) of the comparison analysis (g). (For interpretation of the references to color in this figure legend, the reader is referred to the web version of this article.)

First, individual MRI scans were linearly registered into a standard space (MNI152) by using a FSL software package (Jenkinson et al. 2012). Second, the registered images were segmented into three brain tissue types (the gray matter, white matter and cerebrospinal fluid (CSF)) using a modified Gaussian mixture model (SPM8 packages, http://www.fil.ion.ucl.ac.uk/spm/). A group-wise CSF template was then created by applying the geodesic shooting algorithm (Ashburner and Friston 2011), which learns the minimal deformation from all of the individual CSF segmentations to an averaged template. Third, based on this averaged CSF template, we extracted the ventricular structure by mapping a probability ventricular mask, i.e., the automatic lateral ventricle delIneatioN (ALVIN) binary mask (Kempton et al. 2011), onto the template. A binary ventricular template of our dataset was formed, and ventricular boundaries were visually inspected. The deformation matrices from the estimation of group-wise CSF template were then used to wrap the ventricular template back to the individual space. With a topology preserving level-set method (Han et al. 2003) and marching cubes algorithm (Lorensen and Cline 1987), ventricular surface meshes were reconstructed according to the shape of each individual ventricular volumetric template. Before geometric analysis of these reconstructed ventricular surfaces, we applied a two-step mesh smoothing method (Yi et al. 2016) to remove noise and topologically irregular structures. Fourth, due to the naturally occurring 3-horn shape, the whole ventricular surface was cut into three sub-structures by the holomorphic 1-forms segmentation method (Wang et al. 2010). Fifth, sub-ventricular surfaces were independently registered to standard regular maps, and vertex-wise MMS of deformation fields of the surface registration were estimated on these registered surfaces (Wang et al. 2011; Zhang et al. 2016). These MMS can be regarded as the vertex-wise geometry features. Finally, we conducted vertex-wise statistical analysis of MMS to compare ventricular morphometry differences between CU progressors and CU non-progressors. Expansive directions of these significant ventricular subregions were analyzed using RD statistics and mTBM statistics separately. Additionally, we also make effect size analysis of VV and our proposed MMS measures. The entire ventricular morphometry analysis pipeline is publicly available at http://gsl.lab.asu.edu/software/ventricle/.

2.2.1. MRI registration and ventricle segmentation

With the FSL software package (Jenkinson et al. 2012), T1 MRI images were linearly registered into a standard space (MNI152) to remove the effect of brain size. Then the registered images were parcellated into three brain tissue types (the gray matter, white matter, and CSF) using a modified Guassian mixture model (SPM8 packages, http://www.fil.ion.ucl.ac.uk/spm/) to estimate the tissue type probability of each voxel based on a prior probability map. After doing tissue segmentation for all subjects, we estimated a group-wise CSF template through the geodesic shooting algorithm (Ashburner and Friston 2011), which introduced the minimal distortion of mappings from the source CSF image $f(x)$ to the estimated averaged CSF template $\mu(x)$, e.g., $f(\varphi_1(x)) \to \mu(x)$. Essentially, in the first step, the initial CSF template was set as the mean shape and intensity of the individual CSF tissue images and updated iteratively. During each iteration, the objective function is minimized by a proper initial velocity field υ_0 and the final object function is expressed as:

$$E = \frac{1}{2}\|Lv_0\|^2 + \frac{1}{2\sigma^2}\int_{x\in\omega} |J_1^{\varphi}(x)|\,(f(\varphi_1(x)) - \mu(x))^2 dx \quad (1)$$

where the first term measures the image distortion during the mapping

while the second term evaluates accuracy of the mapping for all voxels. Here, φ_1 is a forward diffeomorphism from subject to template parameterized by υ_0 and $J_1^{\varphi}(x)$ is the corresponding Jacobin tensor. L in the first term is a linear differential operator which can be understood as a regularization of the deformation and is defined as:

$$\|Lv_0\|^2 = \int_{x\in\omega} (\frac{\lambda_1}{4}\|Dv+(Dv)^T\|^2 + \lambda_2 tr(Dv)^2 + \lambda_3\|v\|^2)dx \quad (2)$$

The term associated with λ_1 controls the image shearing and stretching. The term weighted by λ_2 controls local volume expansion and contraction. The last term with λ_3 denotes the absolute displacement of voxels. Details of optimizing Eq. (1) can be found in (Ashburner and Friston 2011). A group average of all deformed shapes is computed after each round of iteration and set as the template for the next iteration. Eventually, a stable result of CSF template is derived after several iterations, e.g. typically 5 to 6 iterations, and is regarded as the group-wise CSF template. As a part of the CSF, the group-wise ventricular template was subsequently obtained by mapping a probability ventricular mask onto the group-wise CSF template. In this study, the Automatic Lateral Ventricle delIneatioN (ALVIN (Kempton et al. 2011)) binary mask was applied to exclude CSF tissues outside the ventricular masks. Once the group-wise ventricular template is extracted, with the help of deformation fields from the previous optimization process, we inversed the image registration and segmented the individual ventricular structures from the original 3D brain images.

2.2.2. Ventricular surface reconstruction and registration

Based on segmented binary volumetric masks, we extracted ventricular boundaries with a topology preserving level-set method (Han et al. 2003) and constructed triangular surface meshes with marching cubes algorithm (Lorensen and Cline 1987). Later, the surfaces were further smoothed using a two-step mesh smoothing method, i.e., combination of "progressive meshes" and Loop subdivision, which had proved to be feature-preserving while effectively reducing the noise and partial volume effect (Yi et al. 2016).

We needed to parameterize the ventricular surface with 2D intrinsic geometry properties (Thompson et al. 2004a; Wang et al. 2011). Since a ventricular surface has a complex geometric structure, i.e., a "multiple-arm" shape, we cut and modeled the whole ventricular surface into three horns using the holomorphic 1-forms method (Wang et al. 2007, 2010). Three horns, including anterior horn, posterior horn and inferior horn, were automatically located and separated from each ventricular surface. This holomorphic 1-forms method induced conformal grids which demonstrated the angle preserving property on the tube-like subregional surfaces (Wang et al. 2007, 2010). Basically, we first followed our previous work (Shi et al. 2015) to locate a singularity point (zero point) which is a geometric landmark of ventricle, and is structurally consistent across subjects. Based on this landmark, a Euclidean conformal parameterization was computed resulting in the 3-horn decomposition. Next, constrained harmonic maps were computed to respectively register each of the ventricular sub-surfaces to a standard map. The harmonic mapping τ can be expressed as below:

$$\tau^{\circ}\tau_1(S_1) = \tau_2(S_2),\ \tau^{\circ}\tau_1(\partial S_1) = \tau_2(\partial S_2),\ \delta\tau = 0 \quad (3)$$

Here τ_1 and τ_2 are conformal parameterizations that respectively map surface S_1 and S_2 to a square disc R^2. The map ϕ from surface S_1 to surface S_2 can be obtained by $\phi = \tau_1{}^{\circ}\tau^{\circ}\tau_2^{-1}$.

2.2.3. Ventricular surface multivariate morphometry statistics (MMS)

Three ventricular horns are tube-like shapes. To improve morphometric analysis, our previous study (Wang et al. 2011) proposed MMS measure to capture differences along all possible directions. MMS consists of RD and mTBM. The RD describes morphometric changes along the surface normal direction (Pizer et al. 1999; Thompson et al. 2004a, b). The mTBM captures deformations within surfaces such as rotation, dilation, and shears with surfaces that are perpendicular to the surface normal direction (Leporé et al. 2008; Wang et al. 2010). After ventricular surface registration and conformal parameterization, RD was defined as the distance from each parametric surface point to the center of 3D positions of the *iso*-u curves (red curves illustrated on ventricular surfaces of Fig. 1) in the parameter domain (Wang et al. 2011).

We calculated the vertex-wise surface mTBMs, which can be represented as a 3×1 feature. MTBM is a "Log-Euclidean metric" (Arsigny et al. 2006) on the set of deformation tensors S, i.e., a 3×1 positive definite matrix ($log(S)$). More specifically, the deformation tensors S is computed as $S = (J^TJ)^{1/2}$, where J is the Jacobian matrix (Wang et al. 2010). Suppose there are two surfaces $A = [a_1, a_2, a_3]$ and $B = [b_1, b_2, b_3]$, which are isometrically embedded on the Euclidean space, the discrete derivative map J from A to B is approximated as $J = [a_3 - a_1, a_2 - a_1][b_3 - b_1, b_2 - b_1]^{-1}$. Eventually, TBM is defined as $\sqrt{\det J}$, where $\det J$ is the determinant of Jacobian matrix and mTBM can be expressed as $\log\sqrt{JJ^T}$. Finally, MMS for each vertex on the individual ventricular surface was formed as a 4×1 vector by combining the mTBM and RD statistics. That is, each individual ventricle can be represented as a $W \times 4$ feature matrix, W is the vertices number of a ventricle surface.

2.2.4. Ventricular surface MMS smoothing

The mesh smoothing process introduced in subsection 2.2.2 is used to reduce the noise from image acquisition, segmentation, and partial volume effects in surface reconstruction (Shi et al. 2013a). The remaining noise and noise introduced in subsequent processes still affect the signal noise ratio (SNR) in the surface features and in the final statistical analysis. Thus, the heat kernel smoothing algorithm (Chung et al. 2005; Shi et al. 2015) was introduced to refine the ventricular surface features. Referring to our previous work (Shi et al. 2015), key parameters of the heat kernel smoothing algorithm were set as: smoothing parameter $\sigma = 1$ and number of iterations $m = 10$.

2.2.5. Group-wise ventricular surface morphometry analysis

The Hotelling's T^2 test (Hotelling 1931; Cao and Worsley 1999) was performed to evaluate the morphometric variations of the smoothed ventricular surfaces between CU progressors and non-progressors on each vertex. Statistical results were corrected for multiple comparisons using the permutation test (Wang et al. 2010). Basically, we calculated the Mahalanobis distance based on the true group labels first. Then we randomly assigned the object surfaces into two groups which had the same number of subjects as in the true group and re-computed the group distance on each surface point. This process repeated 10,000 times with the outcome of 10,000 permutation values on each vertex. A probability (uncorrected p value) on each surface point was computed as a ratio, i.e., percentage of permutations when the estimated permutation values was greater than the true group t value. After that, given a pre-defined statistical threshold, i.e. $p < 0.05$, we defined a feature to be the number of surface points with uncorrected p value lower than this threshold. The feature could be regarded as a real effect in the true experiment, and by comparing it to the features derived from the random groupings, we obtained a ratio that stood for the fraction of the time an effect of similar or greater magnitude to the real effect occurred in the random assignments. This ratio, the *overall (corrected) significance*, provided a global significance level of the map.

After we calculated the significant variations on the ventricular surface, we could apply directional analysis (Yao et al. 2018; Dong et al. 2019) to study the correspondence between VV enlargement and ventricular morphometry expansion. The direction (atrophy or expansion) of group differences were analyzed along the surface normal direction and within surfaces at each surface point. We mapped RD and the determinant of the Jacobian matrix (*detJ*), i.e., the TBM (Davatzikos et al. 1996; Thompson et al. 2000; Chung et al. 2008), at each significant surface vertex k of subject group 1 (CU progressors) and group 2 (CU

non-progressors) in a difference map according to the following formula:

$$R^k = \frac{\sum_i^{N_1} Ver_{1i}^k}{N_1} - \frac{\sum_j^{N_2} Ver_{2j}^k}{N_2} \quad (4)$$

where Ver_{1i}^k and Ver_{2j}^k are the RD or *detJ* for *i*th subject in group 1 and *j*th in group 2, and N_1 and N_2 are the number of subjects in each group. Under the significant level ($p < 0.05$), $R^k > 0$ indicates that CU progressors have an enlargement along the normal direction or within surfaces at a given surface point k contrast to CU non-progressors;$R^k < 0$ indicates that CU progressors have an atrophy along the normal direction or within surfaces at a given surface point k in contrast to CU non-progressors.

2.2.6. Effect size analysis

The effect size method, Cohen's d (Cohen 2013), can determine the degree of ventricular deformations in CU progressors compared to CU non-progressors. Hedge's g is an alternative of Cohen's D where different sample sizes exist, so we use Hedge's g (Eq. (5)) to calculate the effect sizes of ventricular volume measures (Grissom 2014), where m_1 and m_2 are the mean VV values of CD progressor and non-progressor groups respectively, n_1 and n_2 are the sample sizes of each group, SD_1 and SD_2 are the standard deviations of each group. The Hedge's g and Cohen's d statistics can be interpreted by levels: low effect (< 0.5), medium effect (< 0.8) and high effect (> 0.8) (Geuter et al. 2018).

$$Hedges' g = \frac{m_1 - m_2}{SD^*_{pooled}},\ SD^*_{pooled} = \sqrt{\frac{(n_1-1)SD_1^2 + (n_2-1)SD_2^2}{n_1 + n_2 - 2}} \quad (5)$$

MMS is a multivariate measure. The above effect size methods cannot be directly applied. The study of (Sapp et al. 2007) pointed out that Mahalanobis distance can provide a multivariate measure of effect. Within the significant deformation subregions, we make vertex-wise effect size statistics using Mahalanobis distance (Eq. (6)), where M_1 and M_2 are the mean 4 × 1 MMS vector per ventricular surface vertex of CD progressor and non-progressor groups respectively, S is their corresponding 4 × 4 covariance matrix. The Mahalanobis distance D^2 is the multivariate analogue of the univariate Cohen's d effect size, it can be interpreted by levels: small effect (=0.25), medium effect (=0.5) and high effect (> =1) (Stevens 2001).

$$D^2 = (M_1 - M_2)^T S^{-1}(M_1 - M_2) \quad (6)$$

3. Results

3.1. Study samples

Demographic information for the *Arizona APOE* cohort and *ADNI* cohort are summarized in Table 1. Within each cohort, group differences of gender and APOE-ε4 genotype were estimated using chi-square tests, group differences of age and education were calculated by *t*-tests (Crivello et al. 2010; Dong et al. 2019). Inferential analysis demonstrated that the CU progressors and non-progressors have no significant differences on sex, age, education, and relevant APOE genotype.

3.2. Ventricular volume

Since VV measure is an effective measurement for studying AD pathological progress (Jack Jr. et al. 2008; Reiter et al. 2017; Sørensen et al. 2017), we conducted a VV comparison analysis of CU progressors vs. non-progressors using *t*-test on both cohorts. Similar to prior approaches used to compute brain volume for AD diagnosis (Pennanen et al. 2004; Sandstrom et al. 2006; Chupin et al. 2007, 2009; Pardoe et al. 2009), the VVs were computed on the smoothed ventricular structures after they were linearly registered to the MNI imaging space (Patenaude et al. 2011; Shi et al. 2013b). Table 2 shows the volume means (standard deviations) of the CU progressors and non-progressors, at baseline, prior to clinically significant memory decline in the CU progressors. In both cohorts, bilateral VVs of the CU progressors were significantly larger than the non-progressors. Therefore, abnormal enlargements in VVs of CU progressors can be detected two years before a clinically significant memory decline.

Table 1
Demographic characteristics of *Arizona APOE* and *ADNI* cohorts at the time of baseline MRI scan.

	CU progressors	CU non-progressors	*P*-Value
Arizona APOE cohort			
Baseline sample size	n = 18	n = 20	
Sex (M/F)	7/11	7/13	0.80
ε4 Genotype (N)	13:03:02	13:04:03	0.89
% (HM:HT:NC)	(72:17:11)	(65:20:15)	
Age	68.75 ± 4.65	66.76 ± 3.29	0.13
Education	16.44 ± 1.69	15.50 ± 3.33	0.29
ADNI cohort			
Baseline sample size	n = 18	n = 26	
Sex (M/F)	15/3	16/10	0.11
ε4 Genotype (N)(HM:HT:NC)	0:07:11	0:06:20	0.26
Age	79.64 ± 4.16	77.60 ± 3.91	0.10
Education	15.83 ± 3.07	16.62 ± 2.55	0.36

Sex and genotype *p*-values were calculated by chi-squared tests, age and education *p*-values were calculated by *t*-tests. HM = ε4 homozygote; HT = ε4 heterozygote; NC = ε4 non-carrier.

Table 2
Bilateral ventricular volumes of CU progressors and non-progressors at baseline.

	LV volume (cm^3) (mean ± SD)	*p*-value	RV_volume (cm^3) (mean ± SD)	*p*-value
Arizona APOE cohort				
CU progressors	53.6 ± 15.0	0.017	51.8 ± 18.2	0.047
CU non-progressors	42.7 ± 11.8		41.5 ± 10.9	
ADNI cohort				
CU progressors	48.6 ± 10.8	0.018	47.3 ± 11.0	0.013
CU non-progressors	41.2 ± 8.6		39.2 ± 9.5	

Volume values are mean and (SD, standard deviation) when applicable. Volume comparison *p*-values were calculated by *t*-test. LV: left ventricle; RV: right ventricle. CU: cognitively unimpaired.

3.3. Ventricular morphometry

After ventricular abnormalities of CU progressors were detected using the VV measure, we expected to further reveal abnormal subregional expansions on ventricular surfaces of the CU progressors with VMAS. Fig. 2 shows the *p*-maps of CU progressors vs. non-progressors at particular regions of the bilateral ventricles. Non-blue colors show vertices with statistical differences at the nominal 0.05 level, uncorrected for multiple comparisons. In the two independent cohorts, we observed consistent deformation patterns of ventricular subregions in the CU progressors, which were mainly on the anterior horn of both ventricles and more on the left ventricle than the right side. We then reran analyses with a permutation test to correct for multiple comparisons. In the *Arizona APOE* cohort (20 CU non-progressors vs. 18 CU progressors), we found overall significant morphometric differences on the left ventricle (LV, $p = 0.01$) and the right ventricle (RV, $p = 0.03$), as shown in Fig. 2(a). In the *ADNI* cohort (26 CU non-progressors vs. 18 CU progressors), we also found overall significant morphometric differences on the LV ($p = 0.01$) and RV ($p = 0.02$), as shown in Fig. 2(b).

3.4. Directional ventricular morphometry

Additionally, we analyzed the directions of surface deformations

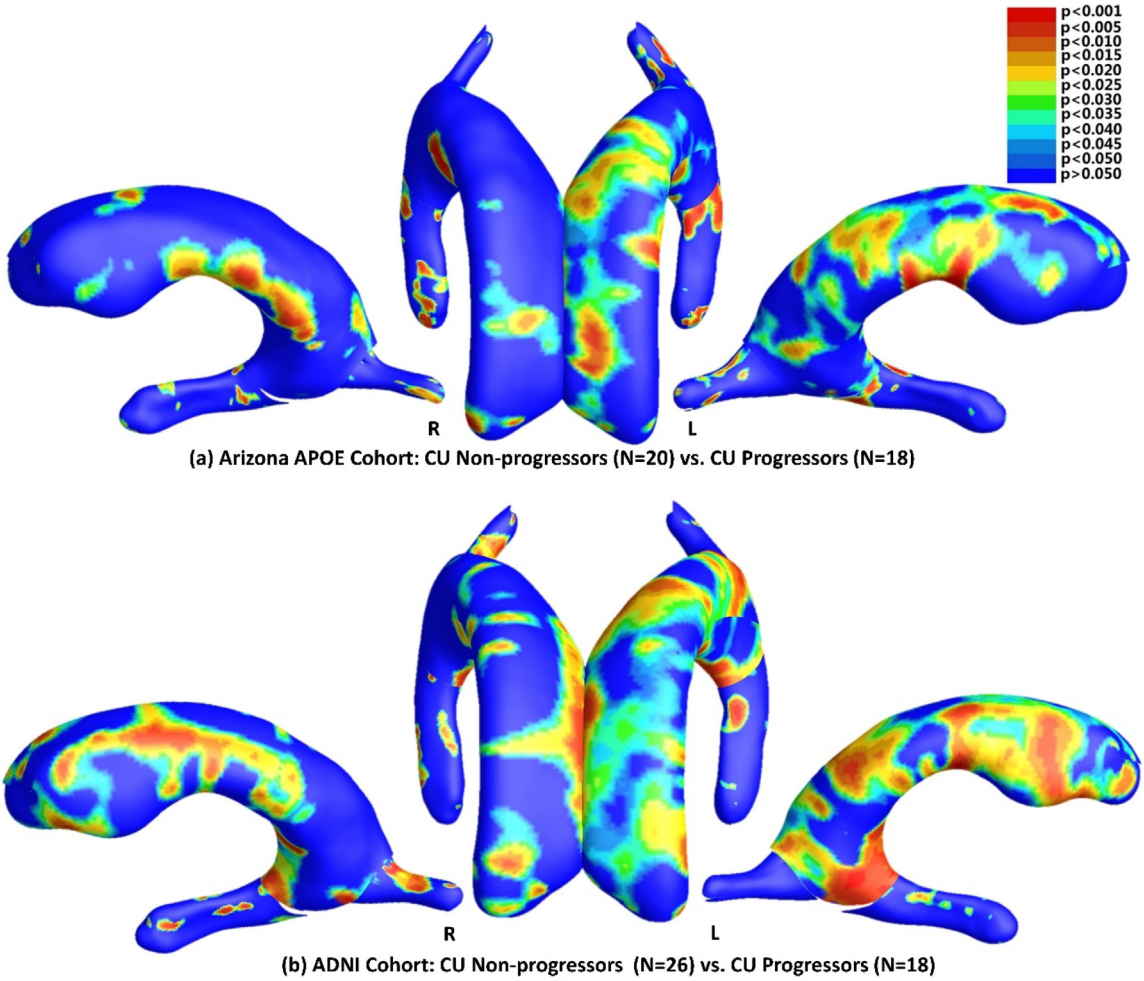

Fig. 2. Subregional differences on the ventricular surfaces of CU progressors and non-progressors in two independent cohorts. Color indicates level of p value, uncorrected, for group comparisons at particular regions. When a permutation test was run to correct for multiple comparisons, for the *Arizona APOE* cohort (a) there were significantly overall morphometric differences between the CU non-progressors and progressors on the left ($p = 0.01$) and right ($p = 0.03$) ventricles; a similar effect was found in the *ADNI* cohort (b, left ventricle, $p = 0.01$, and right ventricle, $p = 0.02$).

using RD and mTBM metrics. Consistent with VV enlargement results, these significantly abnormal ventricular regions of CU progressors are expansive along the normal direction or within surfaces compared to CU non-progressors in both the *Arizona APOE* and *ADNI* cohorts. The studied regions (non-blue areas) in Figs. 3 and 4 are the statistically significant regions from group difference studies shown in Fig. 2(a) and (b). They are identified by using the proposed statistics, i.e. MMS, the combination of RD and mTBM. Here, we extend our observation in a way to emphasize the deformation directions. It is worth noting that the enhanced statistical power gained by additional directional elements in mTBM cannot be visualized by TBM. Even so, within the detected significant regions, RD and mTBM convey a rather similar expansive pattern in most parts, indicated by the fact that most of the red regions are overlapped. Few inverse associations in some (green) regions presented that these regions are atrophy (Figs. 3 and 4a) measured by RD but expansive (Figs. 3 and 4b) measured by TBM, and vice versa. The similarity between panels (a) and (b) in Figs. 3 and 4 helps demonstrate the largely consistent observations from RD and surface TBM, i.e., the expansion along the normal direction (measured by RD) may also result in surface area expansive (measured by TBM). In Fig. 4, these findings were reproduced in ADNI cohort. These directional analyses demonstrated that RD may be a good complement to mTBM. MMS may illustrate the ventricular subregional deformations comprehensively.

3.5. Cumulative distribution analysis of the ventricular morphometry

To further validate which lateral ventricle is more sensitive to the progress of AD pathology, the cumulative distribution functions (CDF) of the contrast p-values are plotted against the corresponding p-value that would be expected, under the null hypothesis of no group difference, as has been used in our prior work (Wang et al. 2010, 2011, 2013; Shi et al. 2013b, 2014; Dong et al. 2019). For null distributions, the CDF of p-values is expected to fall approximately along the line ($y = x$) (Wang et al. 2010). Greater effect sizes are represented by larger deviations (the theory of false discovery rates gives the formulation for thresholds that control false positives at a known rate).

Fig. 5 shows CDF of the p-values from bilateral ventricular morphometry comparisons of CU progressors vs. CU non-progressors in the two cohorts, respectively, plotted against the expected p-values under the null hypothesis (blue dashed line) of no group differences among the comparisons. The deviations of the statistics from the null distribution generally increased from RV abnormalities (green line) to LV abnormalities (red line) in CU subjects, suggesting that the LV has greater effect sizes to track AD pathologic progress in the preclinical stage compared to the RV.

3.6. Effect sizes of VV and MMS measures

Effect sizes of VV analysis is calculated using Eq. (5). Table 3 shows

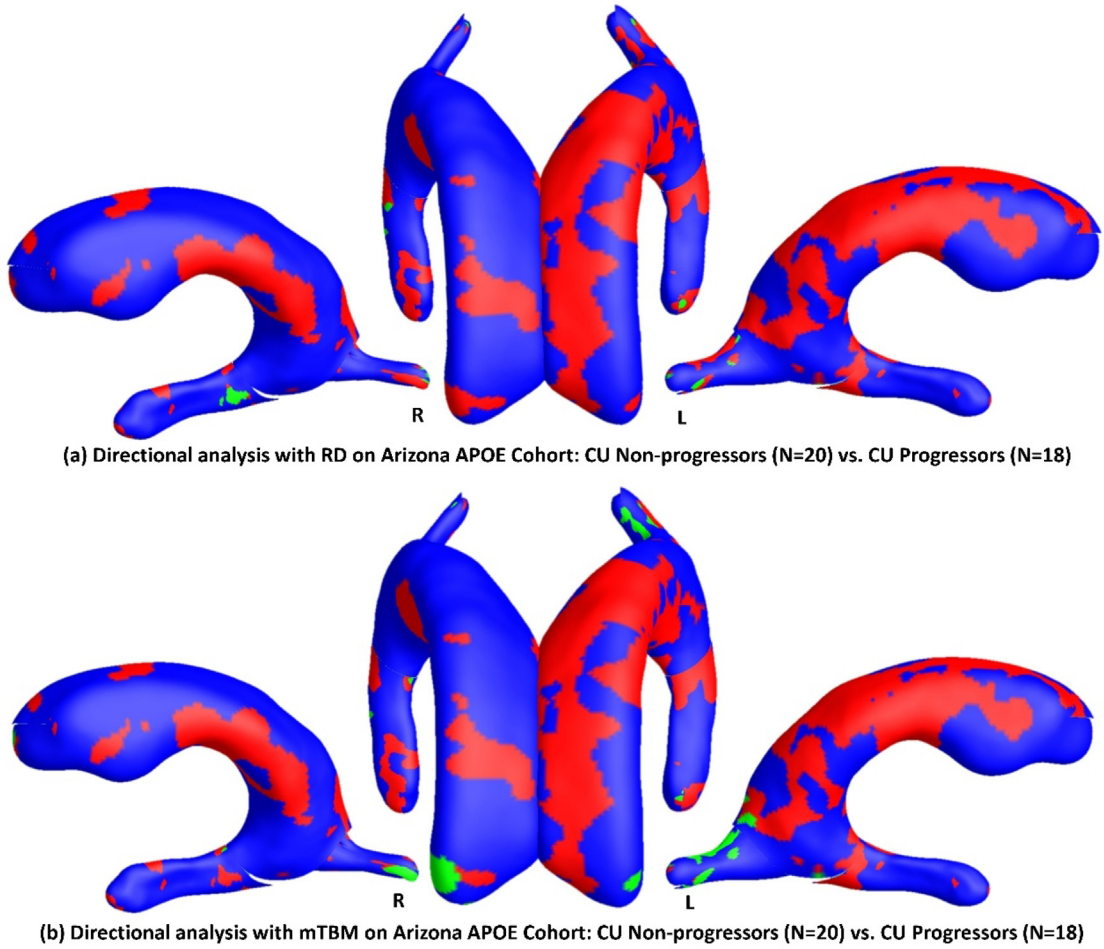

Fig. 3. Directional analysis in non-blue regions ($p < 0.05$) of CU progressors compared to non-progressors in *Arizona APOE* cohort. Red and green colors highlight vertices with significant ventricular expansions and atrophies along the surface normal directions (a) and within surfaces (b), respectively. (For interpretation of the references to color in this figure legend, the reader is referred to the web version of this article.)

the effect sizes of bilateral VV comparisons on two cohorts. VV measure has medium effect sizes (> 0.5 and $< = 0.8$) in distinguishing CU progressors and non-progressors.

Within the significant deformation subregions, effect sizes of MMS comparisons are calculated using Eq. (6). Fig. 6 shows the vertex-wise effect size maps of bilateral MMS comparisons on two cohorts. Most of the effect sizes are > 0.8 (red regions). Yellow subregions represent large ($D^2 = > 1$) effect sizes. These effect size results demonstrate that ventricular MMS has added value compared to VV.

4. Discussion

After analyzing cross-sectional structural MRI images of two independent CU cohorts, our results consistently show that CU progressors have larger ventricular expansions mainly in the anterior horns (greater on the left ventricle) compared to CU non-progressors. These results support our hypothesis that our completely automated VMAS can detect ventricular morphometry abnormalities of CU progressors compared to CU non-progressors prior to clinically significant memory decline. These ventricular morphometric abnormalities did not only mirror VV estimates in two independent cohorts, but they also detailed the abnormal subfields caused by AD. To our knowledge, this is the first study to use the surface-based ventricular morphometry approach to successfully detect ventricular subregional abnormalities of CU progressors two years before their progression to clinically significant memory decline. Our study is among the first to describe a completely automated VMAS capable of generating a whole connected 3D ventricular shape model.

4.1. Ventricular volumetric analysis in cognitively unimpaired subjects

Lateral ventricular boundaries (CSF/brain) have high contrast from adjacent tissue, which facilitates ventricular segmentation in MRI scans, so that ventricular measures may be the most reliable and robust for studying AD pathophysiologic progression (Ferrarini et al. 2008; Chou et al. 2008; Madsen et al. 2013, 2015). Previous studies (Weiner et al. 2015; Madsen et al. 2015; Coupé et al. 2019) demonstrated VV measures can detect ventricular enlargements associated with AD prior to clinically significant memory decline. Here, we estimated the VV differences between CU progressors and non-progressors in two independently CU cohorts. Our results are consistent with those of previous studies (Weiner 2008; Coupé et al. 2019), showing that abnormal ventricular expansions are prior to future clinically cognitive decline in CU progressors. This knowledge will facilitate subject enrollment, in a timely fashion, in clinical trials aimed at prevention of AD process (Jack et al. 2004; Weiner 2008; Apostolova et al. 2012; Roussotte et al. 2014a; Madsen et al. 2015; Coupé et al. 2019). Additionally, our results from two cognitively unimpaired cohorts indicate the left ventricle volume is larger than the right, so we infer that the left ventricle is more severely affected than the right during the pre-clinical stage. Consistent with this, others have found a larger left VV in MCI patients compared to CUs (Apostolova et al. 2012; Madsen et al. 2015).

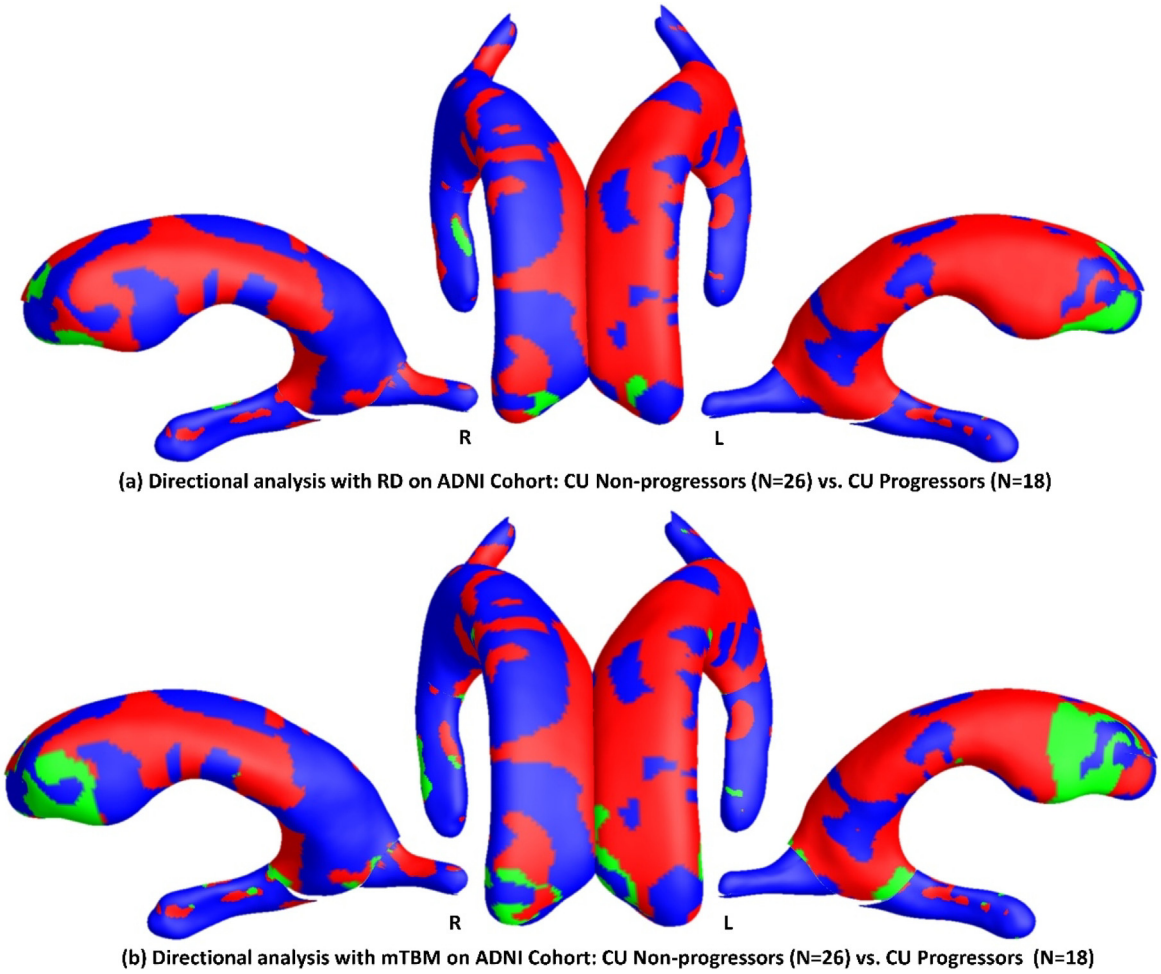

Fig. 4. Directional analysis in non-blue regions ($p < 0.05$) of CU progressors compared to non-progressors in *ADNI* cohort. Red and green colors highlight vertices with significant ventricular expansions and atrophies along the surface normal directions (a) and within surfaces (b), respectively. (For interpretation of the references to color in this figure legend, the reader is referred to the web version of this article.)

4.2. Ventricular shape modeling in cognitively unimpaired subjects

It is difficult to parameterize the ventricular surface because of its 'multiple-arm' structural property (Wang et al. 2010). To capture more deformation details of the ventricular structure, some studies developed surface-based ventricular morphometry analysis methods based on RD measures to track deformations roughly along the surface normal direction, and found anterior and body/posterior horn portions of the lateral ventricles had age-related expansions (Thompson et al. 2004a; Apostolova et al. 2012). Other studies developed TBM-based methods to track ventricular deformations within surfaces (Thompson et al. 2007; Hua et al. 2008; Shi et al. 2015), the study of (Shi et al. 2015) applied the TBM biomarker to distinguish ventricular shapes of 71 MCI converters from 62 MCI stable controls, and these group different regions close to the temporal lobe and posterior cingulate. Our previous study (Wang et al. 2011) indicated mTBM provided better effect sizes for detecting ventricular morphometric differences than TBM measure in 804 subjects (184 CE, 391 MCI and 229 CU). The proposed VMAS applied MMS including RD and mTBM to detect abnormal deformations along the ventricular surface normal directions and within the ventricular surfaces of CU progressors, which have not been extensively studied. Our results demonstrated that pre-symptomatic CU progressors have more expansive ventricular anterior subfields, and the left ventricle is more prominent in this regard than the right.

To our knowledge, it is the first study to use the surface-based ventricular morphometry approach to successfully identify ventricular abnormalities in pre-symptomatic CU progressors. Several brain imaging-based AD studies (Thompson et al. 2004b; Styner et al. 2005; Ferrarini et al. 2008; Chou et al. 2009; Morra et al. 2009; Apostolova et al. 2010; Costafreda et al. 2011) demonstrated that surface-based biomarkers outperform volume measures. Regional brain deformations associated with AD involve wide range of brain structures, the well-known structures are hippocampus, ventricle and cortical thickness (Frisoni et al. 2010; Cuingnet et al. 2011; Pettigrew et al. 2016; Reiter et al. 2017; Sørensen et al. 2017). Together with this work, we developed a series of surface-based biomarkers of different brain structures for AD research (Wang et al. 2010, 2011; Fan et al. 2018; Dong et al. 2019). Our latest work (Dong et al. 2020) has indicated that combining these three biomarkers could empower the prediction of AD progression. The current work also lays down a solid foundation for our future comprehensive AD structural biomarkers in the preclinical stage. Additionally, previous studies of ventricular morphometric modeling (Apostolova et al., 2012; Chou et al., 2008; Ferrarini et al., 2008; Roussotte et al., 2014; Thompson et al., 2004; Wang et al., 2011, 2013) mapped only part of anatomical ventricular surfaces, with coverage of inferior or posterior horns being incomplete. This work proposes an automated ventricular surface segmentation method which can generate a whole connected 3D ventricular model, which benefits tracking more ventricular subregional information.

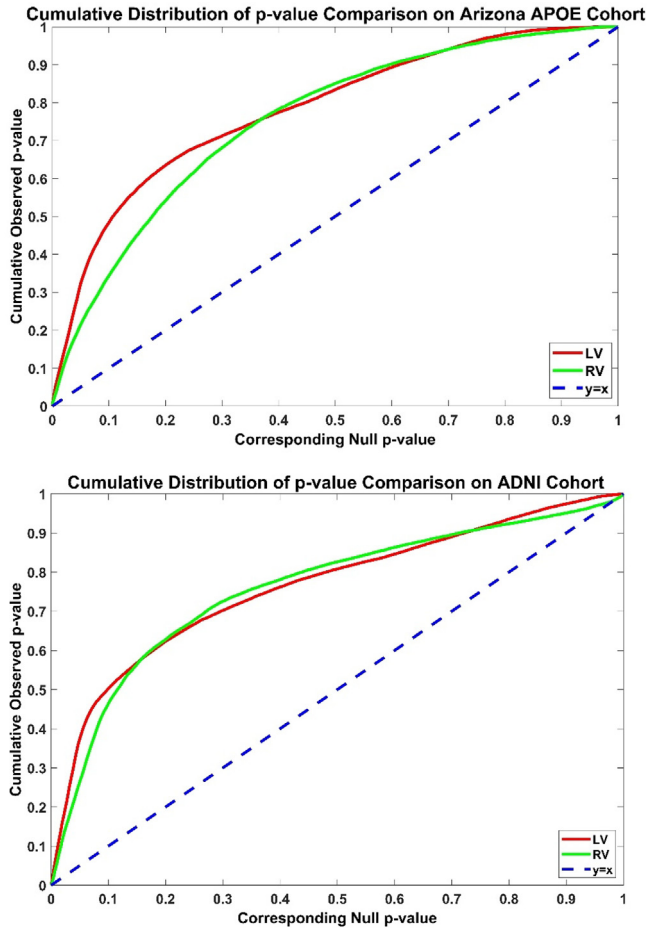

Fig. 5. Cumulative distribution functions of the *p*-values from bilateral ventricular morphometry comparisons of CU progressors vs. non-progressors in two independent cohorts, plotted against the expected *p*-values under the null hypothesis (y = x, blue dash line) of no group differences among the comparisons. In the false discovery rate methods, any cumulative distribution plot that rises steeply is a sign of a significant signal being detected, with curves that rise faster denoting higher effect sizes. The steep rise of the cumulative plot relative to *p*-values that would be expected by chance can be used to compare the detection sensitivity of different statistics derived from the same data. The deviations of the statistics from the null distribution generally increased from right ventricle (RV) abnormalities (green line) to left ventricle (LV) abnormalities (red line) in the CU subjects, suggesting that the LV is more sensitive to AD pathologic progress in the preclinical stage compared to the RV. (For interpretation of the references to color in this figure legend, the reader is referred to the web version of this article.)

Table 3
Effect sizes of ventricular volumes of CU progressors and non-progressors at baseline.

	LV volume effect size	RV volume effect size
Arizona APOE cohort		
CU progressors vs. CU non-progressors	0.738	0.700
ADNI cohort		
CU progressors vs. CU non-progressors	0.774	0.800

Effect size values were calculated by Hedges' g. LV: left ventricle; RV: right ventricle. CU: cognitively unimpaired.

4.3. Limitations and future work

Despite the promising results are obtained by applying our automated VMAS on MRIs of CU progressors and non-progressors, there are three important caveats. First, this work used limited sample sizes to estimate ventricular morphometry abnormalities of CU progressors. We will further validate our algorithm in other large brain image cohorts, such as ADNI-2 (Jack et al. 2015), UK Biobank (Sudlow et al. 2015) and Adolescent Brain Cognitive Development (ABCD) study (Jernigan and Brown 2018). And we will apply VMAS to compare and correlate with other well-known biomarkers like amyloid-status (Wu et al. 2018) and tau PET biomarkers (Brier et al. 2016; Gordon et al. 2019). Second, due to the age difference in two cohorts, the identified expansive regions across cohorts are not identical. We can observe extended significantly different areas in the elder ADNI cohort. It may indicate that the increased enlargement areas in the elder CU progressor group. The study of (Worker et al. 2018) applied the linear mixed effects model to track the sensitive hippocampal subregion univariate volume differences in CU and AD populations. In future work, to suppress cohort heterogeneity and keep the general deformation subregions, we will explore the linear mixed effects model (Avilés 2001; Worker et al. 2018) on multivariate morphometry statistics. Third, VMAS integrated RD and mTBM for improved statistical power. The current RD computation relies on surface conformal parameterization and on *iso*-u curves (Wang et al. 2011). Our recent work (Mi et al. 2018) proposed a novel method to compute regularized Wasserstein means. The computed Wasserstein means of surface is a skeleton which carries global shape information. Therefore, the radial distance defined on the Wasserstein means may be more robust and accurate. Our future work will integrate the robust RD estimate method (Mi et al. 2018) into the VMAS. We expect that by combining the new RD statistical method and mTBM, the VMAS may gain more statistical power at detecting localized ventricular anatomical expansions of CU progressors.

5. Conclusion

This work proposed a novel automated ventricular morphometry analysis system. There are several advantages of this system. First, the individual ventricle mask is derived from a common template which reflects common and special ventricular structural variations. Second, it generates a whole connected 3D ventricular shape model which benefits the surface-based morphometric analysis. Finally, it works on an automated pipeline, without subjective interventions during the process. The VMAS was test-retested on two independent cognitively unimpaired cohorts, and showed that ventricular morphometric abnormalities of the CU progressors can be detected prior to imminent progression to clinically significant memory decline, with LV surface statistics presenting higher effect sizes than RV.

CRediT authorship contribution statement

Qunxi Dong: Methodology, Software, Investigation, Writing - original draft. **Wen Zhang:** Methodology, Software, Investigation, Writing - original draft. **Cynthia M. Stonnington:** Conceptualization, Resources, Data curation. **Jianfeng Wu:** Methodology, Software, Investigation, Writing - original draft. **Boris A. Gutman:** Software. **Kewei Chen:** Conceptualization, Resources, Data curation. **Yi Su:** Conceptualization, Resources, Data curation. **Leslie C. Baxter:** Conceptualization, Resources, Data curation. **Paul M. Thompson:** Conceptualization, Resources, Supervision. **Eric M. Reiman:** Conceptualization, Resources, Supervision. **Richard J. Caselli:** Conceptualization, Investigation, Writing - review & editing, Supervision. **Yalin Wang:** Conceptualization, Investigation, Writing - review & editing, Supervision.

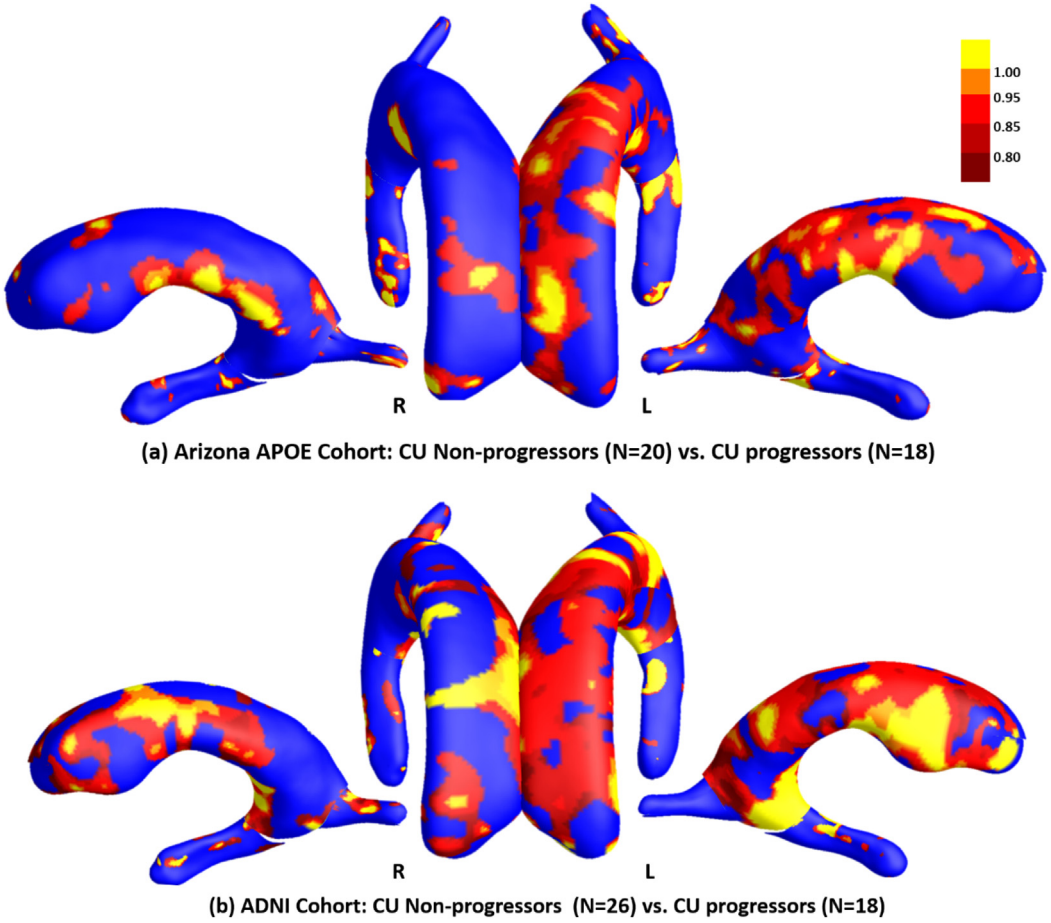

Fig. 6. Illustrations of the effect size maps of CU progressors compared to non-progressors in *Arizona APOE cohort* and *ADNI* cohort.

Acknowledgements

Algorithm development and image analysis for this study was funded, in part, by the National Institute on Aging (R21AG043760 to RJC and YW; RF1AG051710 to QD, WZ, JW, PMT, and YW; R01AG031581 and P30AG19610 to EMR and RJC); the National Institute of Biomedical Imaging and Bioengineering (R01EB025032 to WZ, JW, and YW; U54EB020403 to BAG, PMT, WZ, JW, and YW); and the Arizona Alzheimer's Consortium (CMS, WZ, JW, YS, KC, LCB, EMR, RJC, and YW).

Part of data collection and sharing for this project was funded by the ADNI (National Institutes of Health Grant U01 AG024904), and DOD ADNI (Department of Defense award number W81XWH-12-2-0012). ADNI is funded by the National Institute on Aging, the National Institute of Biomedical Imaging and Bioengineering, and through generous contributions from the following: AbbVie, Alzheimer's Association; Alzheimer's Drug Discovery Foundation; Araclon Biotech; BioClinica, Inc.; Biogen; Bristol-Myers Squibb Company; CereSpir, Inc.; Cogstate; Eisai Inc.; Elan Pharmaceuticals, Inc.; Eli Lilly and Company; EuroImmun; F. Hoffmann-La Roche Ltd and its affiliated company Genentech, Inc.; Fujirebio; GE Healthcare; IXICO Ltd.; Janssen Alzheimer Immunotherapy Research & Development, LLC.; Johnson & Johnson Pharmaceutical Research & Development LLC.; Lumosity; Lundbeck; Merck & Co., Inc.; Meso Scale Diagnostics, LLC.; NeuroRx Research; Neurotrack Technologies; Novartis Pharmaceuticals Corporation; Pfizer Inc.; Piramal Imaging; Servier; Takeda Pharmaceutical Company; and Transition Therapeutics. The Canadian Institutes of Health Research is providing funds to support ADNI clinical sites in Canada. Private sector contributions are facilitated by the Foundation for the National Institutes of Health (www.fnih.org). The grantee organization is the Northern California Institute for Research and Education, and the study is coordinated by the Alzheimer's Therapeutic Research Institute at the University of Southern California. ADNI data are disseminated by the Laboratory for Neuro Imaging at the University of Southern California.

References

Albert, M.S., DeKosky, S.T., Dickson, D., et al., 2011. The diagnosis of mild cognitive impairment due to Alzheimer's disease: Recommendations from the National Institute on Aging-Alzheimer's Association workgroups on diagnostic guidelines for Alzheimer's disease. Alzheimer's Dement 7, 270–279. https://doi.org/10.1016/j.jalz.2011.03.008.

Apostolova, L.G., Green, A.E., Babakchanian, S., et al., 2012. Hippocampal atrophy and ventricular enlargement in normal aging, mild cognitive impairment (MCI), and Alzheimer disease. Alzheimer Dis. Assoc. Disord. 26, 17–27. https://doi.org/10.1097/WAD.0b013e3182163b62.

Apostolova, L.G., Morra, J.H., Green, A.E., et al., 2010. Automated 3D mapping of baseline and 12-month associations between three verbal memory measures and hippocampal atrophy in 490 ADNI subjects. Neuroimage 51, 488–499. https://doi.org/10.1016/j.neuroimage.2009.12.125.

Arsigny, V., Fillard, P., Pennec, X., Ayache, N., 2006. Log-Euclidean Metrics for Fast and Simple Calculus on Diffusion Tensors. Magn. Reson. Med. 56, 411–421.

Ashburner, J., Friston, K.J., 2011. Diffeomorphic registration using geodesic shooting and Gauss-Newton optimisation. Neuroimage 55, 954–967. https://doi.org/10.1016/j.neuroimage.2010.12.049.

Avilés, A.I., 2001. Linear Mixed Models for Longitudinal Data. Technometrics. https://doi.org/10.1198/tech.2001.s630.

Brier, M.R., Gordon, B., Friedrichsen, K., et al., 2016. Tau and Ab imaging, CSF measures, and cognition in Alzheimer's disease. Sci. Transl. Med. 8, 1–10. https://doi.org/10.1126/scitranslmed.aaf2362.

Brookmeyer, R., Johnson, E., Ziegler-Graham, K., Arrighi, H.M., 2007. Forecasting the global burden of Alzheimer's disease. Alzheimer's Dement 3, 186–191. https://doi.org/10.1016/j.jalz.2007.04.381.

Cao, J., Worsley, K.J., 1999. The detection of local shape changes via the geometry of Hotelling's T2 fields. Ann. Stat. 27, 925–942.

Cardenas, V.A., Chao, L.L., Studholme, C., et al., 2011. Brain atrophy associated with

baseline and longitudinal measures of cognition. Neurobiol. Aging 32, 572–580.
Caselli, R.J., Dueck, A.C., Osborne, D., et al., 2009. Longitudinal modeling of age-related memory decline and the APOE epsilon4 effect. N. Engl. J Med. 361, 255–263. https://doi.org/10.1056/NEJMoa0809437.
Caselli, R.J., Reiman, E.M., Osborne, D., et al., 2004. Longitudinal changes in cognition and behavior in asymptomatic carriers of the APOE e4 allele. Neurology 62, 1990–1995.
Chen, K., Reiman, E.M., Alexander, G.E., et al., 2007. Correlations between apolipoprotein E epsilon4 gene dose and whole brain atrophy rates. Am. J. Psychiatry. 164, 916–921. https://doi.org/10.1176/ajp.2007.164.6.916.
Chou, Y.-Y., Leporé, N., de Zubicaray, G.I., et al., 2008. Automated ventricular mapping with multi-atlas fluid image alignment reveals genetic effects in Alzheimer's disease. Neuroimage 40, 615–630. https://doi.org/10.1016/j.neuroimage.2007.11.047.
Chou, Y.-Y., Leporé, N., Saharan, P., et al., 2010. Ventricular maps in 804 ADNI subjects: correlations with CSF biomarkers and clinical decline. Neurobiol Aging 31, 1386–1400. https://doi.org/10.1016/j.neurobiolaging.2010.05.001.
Chou, Y.Y., Leporé, N., Avedissian, C., et al., 2009. Mapping correlations between ventricular expansion and CSF amyloid and tau biomarkers in 240 subjects with Alzheimer's disease, mild cognitive impairment and elderly controls. Neuroimage 46, 394–410. https://doi.org/10.1016/j.neuroimage.2009.02.015.
Chung, M.K., Dalton, K.M., Davidson, R.J., 2008. Tensor-Based Cortical Surface Morphometry via Weighted Spherical Harmonic Representation. IEEE Trans. Med. Imaging. 27, 1143–1151. https://doi.org/10.1109/TMI.2008.918338.
Chung, M.K., Robbins, S.M., Dalton, K.M., et al., 2005. Cortical thickness analysis in autism with heat kernel smoothing. Neuroimage 25, 1256–1265. https://doi.org/10.1016/j.neuroimage.2004.12.052.
Chung, MK, Worsley, KJ, Evans, AC, 2003. Tensor-based brain surface modeling and analysis. In: 2003 IEEE Computer Society Conference on Computer Vision and Pattern Recognition, 2003. Proceedings. IEEE Comput. Soc pp I-467-I–473. IEEE Comput. Soc.
Chupin, M., Gerardin, E., Cuingnet, R., et al., 2009. Fully automatic hippocampus segmentation and classification in Alzheimer's disease and mild cognitive impairment applied on data from ADNI. Hippocampus 19, 579–587. https://doi.org/10.1002/hipo.20626.
Chupin, M., Mukuna-Bantumbakulu, A.R., Hasboun, D., et al., 2007. Anatomically constrained region deformation for the automated segmentation of the hippocampus and the amygdala: Method and validation on controls and patients with Alzheimer's disease. Neuroimage 34, 996–1019. https://doi.org/10.1016/j.neuroimage.2006.10.035.
Cohen, J., 2013. Statistical Power Analysis for the Behavioral Sciences. Routledge.
Costafreda, S.G., Dinov, I.D., Tu, Z., et al., 2011. Automated hippocampal shape analysis predicts the onset of dementia in mild cognitive impairment. Neuroimage 56, 212–219.
Coupé, P., Manjón, J.V., Lanuza, E., Catheline, G., 2019. Lifespan Changes of the Human Brain In Alzheimer's Disease. Sci Rep 9, 3998. https://doi.org/10.1038/s41598-019-39809-8.
Crivello, F., Lemaître, H., Dufouil, C., et al., 2010. Effects of ApoE-ε4 allele load and age on the rates of grey matter and hippocampal volumes loss in a longitudinal cohort of 1186 healthy elderly persons. Neuroimage 53, 1064–1069. https://doi.org/10.1016/j.neuroimage.2009.12.116.
Cuingnet, R., Gerardin, E., Tessieras, J., et al., 2011. Automatic classification of patients with Alzheimer's disease from structural MRI: A comparison of ten methods using the ADNI database. Neuroimage 56, 766–781. https://doi.org/10.1016/j.neuroimage.2010.06.013.
Davatzikos, C., Vaillant, M., Resnick, S.M., et al., 1996. A computerized approach for morphological analysis of the corpus callosum. J. Comput. Assist. Tomogr. 20, 88–97.
Dong, Q., Zhang, J., Li, Q., et al., 2020. Integrating Convolutional Neural Networks and Multi-Task Dictionary Learning for Cognitive Decline Prediction with Longitudinal Images. J. Alzheimer's Dis 75, 971–992. https://doi.org/10.3233/JAD-190973.
Dong, Q., Zhang, W., Wu, J., et al., 2019. Applying surface-based hippocampal morphometry to study APOE-E4 allele dose effects in cognitively unimpaired subjects. NeuroImage. Clin. 22, 101744. https://doi.org/10.1016/j.nicl.2019.101744.
Fan Y, Wang G, Lepore N, Wang Y (2018) A tetrahedron-based heat flux signature for cortical thickness morphometry analysis. In: Lecture Notes in Computer Science (including subseries Lecture Notes in Artificial Intelligence and Lecture Notes in Bioinformatics).
Ferrarini, L., Palm, W.M., Olofsen, H., et al., 2006. Shape differences of the brain ventricles in Alzheimer's disease. Neuroimage 32, 1060–1069. https://doi.org/10.1016/j.neuroimage.2006.05.048.
Ferrarini, L., Palm, W.M., Olofsen, H., et al., 2008. MMSE scores correlate with local ventricular enlargement in the spectrum from cognitively normal to Alzheimer disease. Neuroimage 39, 1832–1838. https://doi.org/10.1016/j.neuroimage.2007.11.003.
Frisoni, G.B., Fox, N.C., Jack, C.R., et al., 2010. The clinical use of structural MRI in Alzheimer disease. Nat. Rev. Neurol. 6, 67–77. https://doi.org/10.1038/nrneurol.2009.215.
Geuter S, Qi G, Welsh RC, et al (2018) Effect size and power in fMRI group analysis. bioRxiv 1–23. doi: 10.1101/295048.
Gordon, B.A., Blazey, T.M., Christensen, J., et al., 2019. Tau PET in autosomal dominant Alzheimer's disease: Relationship with cognition, dementia and other biomarkers. Brain 142, 1063–1076. https://doi.org/10.1093/brain/awz019.
Grissom, R.J., 2014. Effect Sizes for Research. Routledge.
Gutman, B.A., Hua, X., Rajagopalan, P., et al., 2013. Maximizing power to track Alzheimer's disease and MCI progression by LDA-based weighting of longitudinal ventricular surface features. Neuroimage 70, 386–401. https://doi.org/10.1016/j.neuroimage.2012.12.052.
Han, X., Xu, C., Prince, J.L., 2003. A topology preserving level set method for geometric deformable models. IEEE Trans. Pattern Anal. Mach. Intell. 25, 755–768.
Hotelling, H., 1931. The Generalization of Student's Ratio. Ann Math Stat 2, 360–378. https://doi.org/10.1214/aoms/1177732979.
Hua, X., Lee, S., Hibar, D.P., et al., 2010. Mapping A}lzheimer's disease progression in 1309 {MRI scans: power estimates for different inter-scan intervals. Neuroimage 51, 63–75.
Hua, X., Leow, A.D., Parikshak, N., et al., 2008. Tensor-based morphometry as a neuroimaging biomarker for Alzheimer's disease: An MRI study of 676 AD, MCI, and normal subjects. Neuroimage 43, 458–469. https://doi.org/10.1016/j.neuroimage.2008.07.013.
Jack Jr., C.R., Weigand, S.D., Shiung, M.M., et al., 2008. Atrophy rates accelerate in amnestic mild cognitive impairment. Neurology 70, 1740–1752. https://doi.org/10.1212/01.wnl.0000281688.77598.35.
Jack, C.R., Barnes, J., Bernstein, M.A., et al., 2015. Magnetic resonance imaging in Alzheimer's Disease Neuroimaging Initiative 2. Alzheimer's Dement 11, 740–756. https://doi.org/10.1016/j.jalz.2015.05.002.
Jack, C.R., Bennett, D.A., Blennow, K., et al., 2016. A/T/N: An unbiased descriptive classification scheme for Alzheimer disease biomarkers. Neurology 87, 539–547. https://doi.org/10.1212/WNL.0000000000002923.
Jack, C.R., Shiung, M.M., Gunter, J.L., et al., 2004. Comparison of different MRI brain atrophy rate measures with clinical disease progression in AD. Neurology 62, 591–600. https://doi.org/10.1212/01.WNL.0000110315.26026.EF.
Jenkinson M, Beckmann CF, Behrens TEJ, et al (2012) FSL. Neuroimage 62:782–790. doi: 10.1016/j.neuroimage.2011.09.015.
Jernigan TL, Brown SA (2018) Introduction. Dev Cogn Neurosci 32:1–3. doi: 10.1016/j.dcn.2018.02.002.
Kempton, M.J., Underwood, T.S.A., Brunton, S., et al., 2011. A comprehensive testing protocol for MRI neuroanatomical segmentation techniques: Evaluation of a novel lateral ventricle segmentation method. Neuroimage 58, 1051–1059. https://doi.org/10.1016/j.neuroimage.2011.06.080.
Leporé, N., Brun, C., Chou, Y.-Y., et al., 2008. Generalized Tensor-Based Morphometry of HIV/AIDS Using Multivariate Statistics on Deformation Tensors. IEEE Trans Med Imag 27, 129–141.
Li, B., Shi, J., Gutman, B.A., Baxter, L.C., Thompson, P.M., Caselli, R.J., Wang, Y., 2016. Alzheimer's Disease Neuroimaging, I. Influence of APOE genotype on hippocampal atrophy over time - an N = 1925 surface-based ADNI study. PLoS One 11 (4), e0152901.
Li, S., Yuan, X., Pu, F., et al., 2014. Abnormal changes of multidimensional surface features using multivariate pattern classification in amnestic mild cognitive impairment patients. J Neurosci 34, 10541–10553. https://doi.org/10.1523/JNEUROSCI.4356-13.2014.
Lorensen WE, Cline HE (1987) Marching cubes: A high resolution 3D surface construction algorithm. In: ACM siggraph computer graphics. pp 163–169.
Madsen SK, Gutman BA, Joshi SH, et al (2013) Mapping Dynamic Changes in Ventricular Volume onto Baseline Cortical Surfaces in Normal Aging, MCI, and Alzheimer's Disease. In: Lecture Notes in Computer Science (including subseries Lecture Notes in Artificial Intelligence and Lecture Notes in Bioinformatics). pp 84–94.
Madsen, S.K., Gutman, B.A., Joshi, S.H., et al., 2015. Mapping ventricular expansion onto cortical gray matter in older adults. Neurobiol Aging 36, S32–S41. https://doi.org/10.1016/j.neurobiolaging.2014.03.044.
McKhann, G.M., Knopman, D.S., Chertkow, H., et al., 2011. The diagnosis of dementia due to Alzheimer's disease: Recommendations from the National Institute on Aging-Alzheimer's Association workgroups on diagnostic guidelines for Alzheimer's disease. Alzheimer's Dement 7, 263–269. https://doi.org/10.1016/j.jalz.2011.03.005.
Mi L, Zhang W, Gu X, Wang Y (2018) Variational Wasserstein Clustering. In: Proceedings of the European Conference on Computer Vision (ECCV). pp 336–352.
Morra, J.H., Tu, Z., Apostolova, L.G., et al., 2009. Automated 3D mapping of hippocampal atrophy and its clinical correlates in 400 subjects with Alzheimer's disease, mild cognitive impairment, and elderly controls. Hum Brain Mapp 30, 2766–2788. https://doi.org/10.1002/hbm.20708.
Pardoe, H.R., Pell, G.S., Abbott, D.F., Jackson, G.D., 2009. Hippocampal volume assessment in temporal lobe epilepsy: How good is automated segmentation? Epilepsia 50, 2586–2592. https://doi.org/10.1111/j.1528-1167.2009.02243.x.
Patenaude, B., Smith, S.M., Kennedy, D.N., Jenkinson, M., 2011. A Bayesian model of shape and appearance for subcortical brain segmentation. Neuroimage 56, 907–922. https://doi.org/10.1016/j.neuroimage.2011.02.046.
Pennanen, C., Kivipelto, M., Tuomainen, S., et al., 2004. Hippocampus and entorhinal cortex in mild cognitive impairment and early AD. Neurobiol Aging 25, 303–310. https://doi.org/10.1016/S0197-4580(03)00084-8.
Pettigrew, C., Soldan, A., Zhu, Y., et al., 2016. Cortical thickness in relation to clinical symptom onset in preclinical AD. NeuroImage Clin 12, 116–122. https://doi.org/10.1016/j.nicl.2016.06.010.
Pizer, S., Fritsch, D., Yushkevich, P., et al., 1999. Segmentation, registration, and measurement of shape variation via image object shape. IEEE Trans Med Imag 18, 851–865.
Reiman, E.M., Uecker, A., Caselli, R.J., et al., 1998. Hippocampal volumes in cognitively normal persons at genetic risk for {A}lzheimer's disease. Ann Neurol 44, 288–291.
Reiter, K., Nielson, K.A., Durgerian, S., et al., 2017. Five-Year Longitudinal Brain Volume Change in Healthy Elders at Genetic Risk for Alzheimer's Disease. J Alzheimer's Dis 55, 1363–1377. https://doi.org/10.3233/JAD-160504.
Roussotte, F.F., Gutman, B.A., Madsen, S.K., et al., 2014a. The apolipoprotein E epsilon 4 allele is associated with ventricular expansion rate and surface morphology in dementia and normal aging. Neurobiol Aging 35, 1309–1317. https://doi.org/10.1016/j.neurobiolaging.2013.11.030.
Roussotte, F.F., Gutman, B.A., Madsen, S.K., et al., 2014b. Combined effects of Alzheimer

risk variants in the CLU and ApoE genes on ventricular expansion patterns in the elderly. J. Neurosci 34, 6537–6545. https://doi.org/10.1523/JNEUROSCI.5236-13.2014.

Saeed, U., Mirza, S.S., MacIntosh, B.J., et al., 2018. APOE-epsilon4 associates with hippocampal volume, learning, and memory across the spectrum of Alzheimer's disease and dementia with Lewy bodies. Alzheimers Dement 14, 1137–1147. https://doi.org/10.1016/j.jalz.2018.04.005.

Sandstrom, C.K., Krishnan, S., Slavin, M.J., et al., 2006. Hippocampal atrophy confounds template-based functional MR imaging measures of hippocampal activation in patients with mild cognitive impairment. AJNR Am. J. Neuroradiol 27, 1622–1627.

Sapp, M., Obiakor, F.E., Gregas, A.J., Scholze, S., 2007. Mahalanobis distance: A multivariate measure of effect in hypnosis research. Sleep Hypn 9, 67–70.

Shi, J., Leporé, N., Gutman, B.A., et al., 2014. Genetic influence of apolipoprotein E4 genotype on hippocampal morphometry: An $N = 725$ surface-based Alzheimer's disease neuroimaging initiative study. Hum Brain Mapp. 35, 3903–3918. https://doi.org/10.1002/hbm.22447.

Shi, J., Stonnington, C.M., Thompson, P.M., et al., 2015. Studying ventricular abnormalities in mild cognitive impairment with hyperbolic Ricci flow and tensor-based morphometry. Neuroimage 104, 1–20. https://doi.org/10.1016/j.neuroimage.2014.09.062.

Shi, J., Thompson, P.M., Gutman, B., et al., 2013a. Surface fluid registration of conformal representation: application to detect disease burden and genetic influence on hippocampus. Neuroimage 78, 111–134. https://doi.org/10.1016/j.neuroimage.2013.04.018.

Shi, J., Wang, Y., Ceschin, R., et al., 2013b. A Multivariate Surface-Based Analysis of the Putamen in Premature Newborns: Regional Differences within the Ventral Striatum. PLoS ONE 8, e66736. https://doi.org/10.1371/journal.pone.0066736.

Sørensen, L., Igel, C., Pai, A., et al., 2017. Differential diagnosis of mild cognitive impairment and Alzheimer's disease using structural MRI cortical thickness, hippocampal shape, hippocampal texture, and volumetry. NeuroImage Clin. 13, 470–482. https://doi.org/10.1016/j.nicl.2016.11.025.

Sperling, R.A., Aisen, P.S., Beckett, L.A., et al., 2011a. Toward defining the preclinical stages of Alzheimer's disease: Recommendations from the National Institute on Aging-Alzheimer's Association workgroups on diagnostic guidelines for Alzheimer's disease. Alzheimer's Dement 7, 280–292. https://doi.org/10.1016/j.jalz.2011.03.003.

Sperling, R.A., Jack, C.R., Black, S.E., et al., 2011b. Amyloid-related imaging abnormalities in amyloid-modifying therapeutic trials: Recommendations from the Alzheimer's Association Research Roundtable Workgroup. Alzheimer's Dement 7, 367–385. https://doi.org/10.1016/j.jalz.2011.05.2351.

Stevens, J.P., 2001. Applied Multivariate Statistics for the Social Sciences, Fifth Edition. Routledge.

Stonnington, C.M., Chen, Y., Savage, C.R., et al., 2018. Predicting Imminent Progression to Clinically Significant Memory Decline Using Volumetric MRI and FDG PET. J. Alzheimer's Dis. 63, 603–615. https://doi.org/10.3233/JAD-170852.

Styner, M., Lieberman, J.A., McClure, R.K., et al., 2005. Morphometric analysis of lateral ventricles in schizophrenia and healthy controls regarding genetic and disease-specific factors. Proc. Natl. Acad. Sci. U S A. https://doi.org/10.1073/pnas.0501117102.

Sudlow, C., Gallacher, J., Allen, N., et al., 2015. UK Biobank: An Open Access Resource for Identifying the Causes of a Wide Range of Complex Diseases of Middle and Old Age. PLoS Med. https://doi.org/10.1371/journal.pmed.1001779.

Thompson, P.M., Dutton, R.A., Hayashi, K.M., et al., 2006. 3D mapping of ventricular and corpus callosum abnormalities in HIV/AIDS. Neuroimage 31, 12–23.

Thompson, P.M., Giedd, J.N., Woods, R.P., et al., 2000. Growth patterns in the developing brain detected by using continuum mechanical tensor maps. Nature 404, 190–193.

Thompson, P.M., Hayashi, K.M., De Zubicaray, G.I., et al., 2004a. Mapping hippocampal and ventricular change in Alzheimer disease. Neuroimage 22, 1754–1766. https://doi.org/10.1016/j.neuroimage.2004.03.040.

Thompson, P.M., Hayashi, K.M., Sowell, E.R., et al., 2004b. Mapping cortical change in Alzheimer's disease, brain development, and schizophrenia. Neuroimage 23, S2–S18. https://doi.org/10.1016/j.neuroimage.2004.07.071.

Thompson, P.M., Hayshi, K.M., Dutton, R.A., et al., 2007. Tracking Alzheimer's Disease. Ann. N Y Acad. Sci. 1097, 183–214. https://doi.org/10.1196/annals.1379.017.

Tosun, D., Chen, Y.-F., Yu, P., et al., 2016. Amyloid status imputed from a multimodal classifier including structural MRI distinguishes progressors from nonprogressors in a mild Alzheimer's disease clinical trial cohort. Alzheimer's Dement 12, 977–986. https://doi.org/10.1016/j.jalz.2016.03.009.

Wang, Y., Lui, L.M., Gu, X., et al., 2007. Brain Surface Conformal Parameterization using Riemann Surface Structure. IEEE Trans. Med. Imag. 26, 853–865.

Wang, Y., Song, Y., Rajagopalan, P., et al., 2011. Surface-based TBM boosts power to detect disease effects on the brain: An N = 804 ADNI study. Neuroimage 56, 1993–2010. https://doi.org/10.1016/j.neuroimage.2011.03.040.

Wang, Y., Yuan, L., Shi, J., et al., 2013. Applying tensor-based morphometry to parametric surfaces can improve MRI-based disease diagnosis. Neuroimage 74, 209–230. https://doi.org/10.1016/j.neuroimage.2013.02.011.

Wang, Y., Zhang, J., Gutman, B., et al., 2010. Multivariate tensor-based morphometry on surfaces: Application to mapping ventricular abnormalities in HIV/AIDS. Neuroimage 49, 2141–2157. https://doi.org/10.1016/j.neuroimage.2009.10.086.

Weiner, M.W., 2008. Expanding ventricles may detect preclinical Alzheimer disease. Neurology 70, 824–825. https://doi.org/10.1212/01.wnl.0000304743.72127.cc.

Weiner, M.W., Veitch, D.P., Aisen, P.S., et al., 2015. 2014 Update of the {A}lzheimer's Disease Neuroimaging Initiative: A review of papers published since its inception. Alzheimer's Dement 11, e1–e120.

Worker, A., Dima, D., Combes, A., et al., 2018. Test–retest reliability and longitudinal analysis of automated hippocampal subregion volumes in healthy ageing and Alzheimer's disease populations. Hum. Brain Mapp. 39, 1743–1754. https://doi.org/10.1002/hbm.23948.

Wu J, Zhang J, Shi J, et al (2018) Hippocampus morphometry study on pathology-confirmed Alzheimer's disease patients with surface multivariate morphometry statistics. In: 2018 IEEE 15th International Symposium on Biomedical Imaging (ISBI 2018). IEEE, pp 1555–1559.

Yao, Z., Fu, Y., Wu, J., et al., 2018. Morphological changes in subregions of hippocampus and amygdala in major depressive disorder patients. Brain Imaging Behav. https://doi.org/10.1007/s11682-018-0003-1.

Yi, H.-A., Möller, C., Dieleman, N., et al., 2016. Relation between subcortical grey matter atrophy and conversion from mild cognitive impairment to Alzheimer's disease. J. Neurol. Neurosurg. Psychiatry 87, 425–432. https://doi.org/10.1136/jnnp-2014-309105.

Zhang W, Shi J, Stonnington C, et al (2016) Morphometric analysis of hippocampus and lateral ventricle reveals regional difference between cognitively stable and declining persons. In: 2016 IEEE 13th International Symposium on Biomedical Imaging (ISBI). IEEE, pp 14–18.

Zhou, J., Liu, J., Narayan, V.A., Ye, J., 2013. Modeling disease progression via multi-task learning. Neuroimage 78, 233–248. https://doi.org/10.1016/J.NEUROIMAGE.2013.03.073.